ELSEVIER

Journal of Biomechanics 33 (2000) 299–306

JOURNAL OF BIOMECHANICS

www.elsevier.com/locate/jbiomech

Role of tapering in aortic wave reflection: hydraulic and mathematical model study

Patrick Segers*, Pascal Verdonck

Hydraulics Laboratory, Institute Biomedical Technology, University of Gent, Sint-Pietersnieuwstraat 41, B-9000 Gent, Belgium

Received 13 October 1998; accepted 12 October 1999

Abstract

Pressure and flow have been measured simultaneously at six locations along the aorta of an anatomically correct 1 : 1 scale hydraulic elastic tube model of the arterial tree. Our results suggest a discrete reflection point at the level of the renal arteries based on (i) the quarter-wavelength formula and (ii) the comparison of foot-to-foot (c_{ff}) and apparent phase velocity (c_{app}). However, separation of the pressure wave into an incident and reflected wave at all six locations indicates continuous reflection: a reflected wave is generated at each location as the forward wave passes by. We did a further analysis using a mathematical transmission line model with a simple tapering geometry (length 50 cm, 31 and 11 mm proximal and distal diameter, respectively) for a low (0.32 ml/mmHg), normal (1.6 ml/mmHg) and high (8 ml/mmHg) value of total arterial compliance. Using the quarter-wavelength formula, a discrete reflection point is found at $x = 33$ cm, the level of the renal arteries, independent of the value of total compliance. However, local analysis comparing c_{ff} and c_{app} does not reveal a marked reflection site, and the analysis of incident and reflected waves merely suggests a continuous reflection. We therefore conclude that the measured in vivo aortic wave reflection indices are the result of at least two interacting phenomena: a continuous wave reflection due to tapering, and local reflections arising from branches at the level of the diaphragm. The continuous reflection is hidden in the input impedance pattern. Using the quarter-wavelength formula or the classical wave separation theory, it appears as a reflection coming from a single discrete site, confusingly also located at the level of the diaphragm. Therefore, the quarter-wavelength formula and the linear wave separation theory should be used with caution to identify wave reflection zones in the presence of tapering, i.e., in most mammalian arteries.

Keywords: Wave reflection; Aorta; Modelling; Tapering; Blood pressure

1. Introduction

Arterial wave reflection is an important determinant of pressure wave morphology (Milnor, 1989). Murgo et al. (1980) classify aortic pressure waves (type A, B and C) based on the occurrence of an inflection point in systole. This inflection point arises from the interaction of a forward wave with a reflected wave. For type C waves, it occurs in late systole. With progressing age, or in hypertension, the reflected wave arrives earlier in the cardiac cycle and the inflection point shifts to early systole, creating a shoulder-like ascending aorta wave profile (type A) and higher systolic pressure and left ventricular load (Murgo et al., 1980). As systolic pressure is an important cardiac risk factor (Franklin and Weber, 1994), it is important to know its determinants. This allows a better tracing and follow-up of high risk patients, early detection of cardiovascular disease and the development of more specific and target-oriented pharmacological agents.

Using a linear wave separation theory, the ascending aorta pressure wave can be decomposed into a forward and a backward wave (Westerhof et al., 1972), each component being the resultant of all antegrade and retrograde travelling waves (Berger et al., 1993). This wave separation theory fits within the concept of the arterial system as a uniform tube, with an "effective length", and a single "apparent" reflection site (Campbell et al., 1989). Based on the same theory, one can derive the quarter-wavelength formula which correlates the frequency of the first minimum in the input impedance to the distance to the apparent reflection site.

Murgo et al. (1980) locate a single reflection point at the level of the aorto-iliac bifurcation. However, O'Rourke (1967) states that at least two reflection sites are required to explain aortic wave phenomena: one at

* Corresponding author. Tel.: + 32-9-2643281; fax: + 32-9-2643595.
E-mail address: patrick.segers@navier.rug.ac.be (P. Segers)

0021-9290/00/$ - see front matter
PII: S0021-9290(99)00180-3

the aorto-iliac bifurcation, and a second one closer to the heart, representing the reflections coming from arteries to the head and upper limbs. This is the basis of the asymmetric T-tube model (O'Rourke and Avolio, 1980). More recently, Latham et al. (1985) measured pressure simultaneously at six locations in the human aorta. Analysis of pressure wave propagation and reflection in the time and frequency domain confirms the existence of a second reflection point, but they locate it in the aorta at the level of the renal arteries. Karamanoglu et al. (1994) also stress the impact of the arteries in the abdomen on the pressure wave morphology, and identify these arteries as the major source of reflection.

In this study, we hypothesise that aortic wave reflection indices result from an interaction of continuous wave reflection, due to tapering, and to local reflections. In particular, we focus on comparing the location of the wave reflection site derived via (i) the quarter-wavelength formula and/or the linear wave separation theory and (ii) time and frequency domain analysis of pressure and flow waves along the aorta. We therefore repeated the in vivo measurements of Latham et al. (1985) in a hydraulic model with an averaged anatomy of the arterial tree, including the aorta and the major large elastic peripheral arteries. The wave reflection indices in the hydraulic model are compared to the in vivo findings of Latham et al. Further, a simplified transmission line model of the tapering aorta will be used to clarify the role of aortic taper in the complex wave reflection pattern.

2. Materials and methods

2.1. Hydraulic model description

The hydraulic model is a 1 : 1 scale model of the human left heart and the arterial tree (Fig. 1). The arterial tree is the physical representation of the configuration published by Westerhof et al. (1969) matching the arterial tree of a male subject of 1.75 m and 75 kg. The model consists of 37 handmade tapering tubes with inner diameters down to 2 mm (interosseus). The aorta has a length of 50 cm, with its diameter varying linearly from 31 mm at the aortic valve (31 mm bioprosthesis) to 11 mm at the aorto-iliac bifurcation (bifurcation angle of 40°). The model contains 28 end-arteries and distal peripheral models, simulating the resistive (pierced rubber) and capacitive (adjustable air volume) properties of the

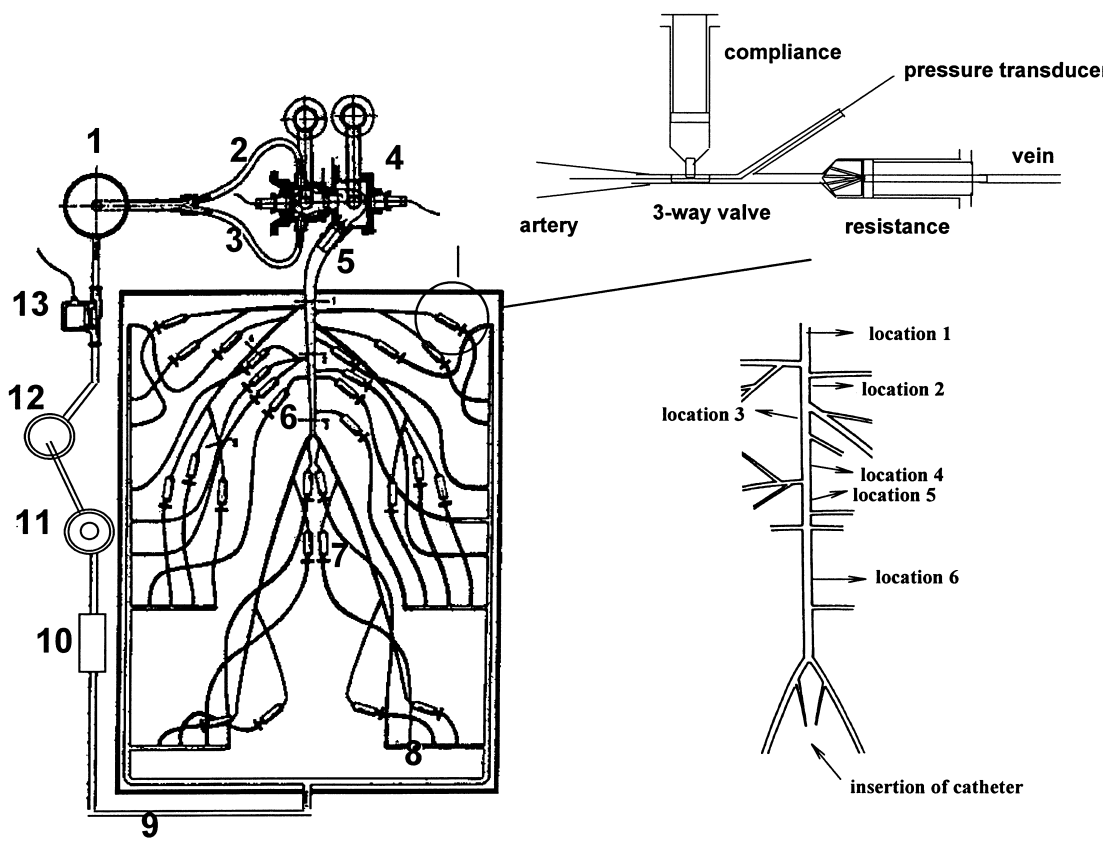

Fig. 1. *Hydraulic model*. Schematic planview drawing of the cardiovascular simulator (left) and the distal peripheral model (upper right). 1: Lung reservoir; 2: pulmonary veins; 3: left atrium; 4: left ventricle; 5: aorta; 6: aorto-iliac bifurcation; 7: peripheral model; 8: veins; 9: venous return conduit; 10: electromagnetic flow meter, 11: venous overflow; 12: buffering reservoir; 13: pump. Bottom right: indication of the six measuring locations along the aorta. (1) Ascending aorta; (2) aortic arch; (3, 4) thoracic aorta; (5, 6) abdominal aorta.

small-sized arteries, arterioles and capillaries (Westerhof et al., 1971). The arterial network is mounted in supine position on a supporting structure and is fixed at discrete locations to avoid bending of the arteries and disturbing oscillations of the arteries. The arteries are not stretched during the experiments. The complete arterial model is submersed in water to allow for ultrasound flow measurements. Total compliance of the model, estimated from pressure–volume measurements, is 0.8 ml/mmHg; total resistance, calculated as the ratio of mean aorta pressure and flow is 1.1 mmHg/(ml/s). The model yields a physiologic input impedance pattern, aortic characteristic impedance (0.054 mmHg/(ml/s) and relevant wave phenomena (wave steepening, systolic rise, wave velocities 6–15 m/s) (Segers et al., 1998).

2.2. Measurements and data analysis

The hydraulic model operates at 60 beats/min with a cardiac output of 4.3 l/min and 122/60 mmHg systolic/diastolic ascending aorta pressure (mean 90 mmHg). Pressure is measured using a catheter tip pressure manometer (Millar, Houston, TX) inserted into the model via the left femoral artery. After positioning the pressure transducer, an ultrasonic flow probe (Transonic, Ithaca, NY), matching aortic dimensions, is mounted around the aorta immediately proximal to the pressure tip transducer. At this location, pressure and flow are measured simultaneously at a sampling rate of 200 Hz (computer A/D card, National Instruments, Texas, USA). Moving the pressure transducer and flow probe, pressure and flow are measured successively at respectively 1, 10, 20, 30, 36 and 48 cm in the arterial network model. At each location, pressure and flow are measured during three consecutive heart beats, and Fourier analysis is applied to this series. Only the first 10 harmonics are taken into account. The input impedance (Z_{in}) is derived at the six locations. Using the frequency of the first minimum of Z_{in} (f_{min}) and the wave velocity (c), the distance to the effective reflecting site (x_{refl}) is derived using the quarter-wavelength formula (Milnor, 1989):

$$x_{refl} = \frac{c}{4 f_{min}}$$

Characteristic impedance (Z_0) is calculated averaging the high frequency components over the frequency range where Z_{in} oscillates around a constant value (Murgo et al., 1980), in our case between 6 and 10 Hz. Pressure is split into an incident or forward wave P_f and a reflected or backward wave P_b using (Westerhof et al., 1972):

$$P_f = \frac{P + Z_0 Q}{2}, \quad P_b = \frac{P - Z_0 Q}{2}.$$

The wave separation is done per harmonic in the frequency domain, and all forward and backward harmonics are added to reconstruct the incident and reflected component in the time domain.

As in Latham et al. (1985), the pressure wave velocity is estimated in two different ways. In the time domain, it is calculated as the propagation speed of the foot of the wave (foot-to-foot wave velocity c_{ff}), the latter obtained from the intersection of straight lines extrapolated from the late diastolic part of the curve and from the steeply rising wave front (Milnor, 1989). In the frequency domain, the apparent phase velocity c_{app} is computed from the phase difference of individual harmonics:

$$c_{app} = \frac{2\pi f \Delta x}{\Delta \varphi}$$

with f the harmonic frequency, Δx the distance between locations and $\Delta\varphi$ the phase difference (Milnor, 1989). The average of the higher frequencies (5–10 Hz) gives $\overline{c_{app}}$ (Latham et al., 1985)

2.3. Mathematical model simulations

The tapering aorta is modelled as a sequence of transmission line model segments (Avolio, 1980; Segers et al., 1997). For each segment, the transmission line equations describe the propagation of pressure (P) and flow (Q) harmonic waves

$$P(x) = P_f e^{-\gamma x} + P_b e^{\gamma x}$$
$$Q(x) = Q_f e^{-\gamma x} + Q_b e^{\gamma x}$$

with x the longitudinal co-ordinate and the subscripts f and b indicating forward and backward waves, respectively. The wave propagation coefficient (γ), accounting for wave propagation and damping, is given as

$$\gamma(\omega) = \frac{i\omega/c_0}{\sqrt{1 - F_{10}}}$$

with F_{10} the Bessel functions as given by Womersley (1957), ω the angular frequency and c_0 the inviscid Moens-Korteweg wave propagation speed given as

$$c_0 = \sqrt{\frac{Eh}{\rho D(1 - \nu^2)}}$$

with E the Young elasticity modulus, h the vessel wall thickness, ρ the blood density (1050 kg/m^3), D the local diameter and ν the Poisson ratio (0.3). The relation between pressure and flow harmonics is given by the characteristic impedance (Z_0) as

$$Z_0 = \frac{P_f}{Q_f} = -\frac{P_b}{Q_b} = \frac{\rho c_0 / A}{\sqrt{1 - F_{10}}}$$

with A the cross-section of the segment. The impedance mismatch between the last segment and the load is explicitly modelled in terms of a reflection coefficient

(Karamanoglu and Fenely, 1997), given by

$$\Gamma = \Gamma_0 e^{-\omega\tau}$$

and with $\Gamma_0 = 0.7$ and $\tau = 0$, yielding a constant and real reflection coefficient. This boundary condition sets the relation $\Gamma = P_b/P_f = -Q_b/Q_f$ at the distal end of the tube.

The upstream boundary condition is a physiological flow wave. Using Fourier analysis, this wave is split into harmonics, and the propagation of individual pressure and flow harmonics over the tube is calculated using the above set of equations. Summation of harmonics finally yields pressure and flow waves in the time domain.

Pressure and flow are calculated in a model for the tapering aorta with a total length of 50 cm. The model is divided into 100 segments of 0.5 cm each, and with diameters varying linearly from 31 mm (upstream diameter) to 11 mm (downstream diameter). Vessel wall thickness is uniform all over the model (0.85 mm). E is constant over the aorta, but three different values are used to yield (i) a low compliance (LC) model with a total compliance of 0.32 ml/mmHg ($E = 2000$ kPa), (ii) a normal compliance (NC) model (1.6 ml/mmHg; $E = 400$ kPa) and (iii) a high compliance (HC) model (8 ml/mmHg; $E = 80$ kPa). Pressure and flow are calculated at the inlet, outlet, and at $x = 30$ cm and are used for the computation of c_{ff} and c_{app}, Z_{in}, Z_0, the distance to the reflection site (x_{refl}), and the incident and reflected wave P_f and P_b. We further vary the number of arterial segments from 2 to 500 (for the HC, NC and LC model) to evaluate the effect on the value of x_{refl}. Finally, the influence of the tapering angle is studied by changing the value of the upstream diameter from 1.1 (0°) to 500 mm (79°). These simulations are again performed for the three models, and with 100 segments.

3. Results

3.1. Hydraulic model measurements

At $x = 1$, the input impedance modulus is 1.26 mmHg/(ml/s) at 0 Hz (total peripheral resistance) and reaches a first minimum of 0.048 mmHg/(ml/s) at 5 Hz. This minimum is accompanied by a phase angle intersecting the x-axis between 5 and 6 Hz (see Segers et al., 1998). Applying the quarter-wavelength formula on the minimum of $|Z_{in}|$ at 5 Hz with a wave velocity of 8 m/s (in the proximal aorta), a distance of 40 cm to the apparent reflection site is found. This location is situated distal to location 5, at the level of the renal arteries.

The foot-to-foot wave velocity c_{ff} increases over the aorta from about 8 m/s in the thorax to 13 m/s in the abdomen (Fig. 2). $\overline{c_{app}}$ is 6–8 m/s in the thorax. It is maximal (27 m/s) between locations 4 and 5 (level of the diaphragm). Below the diaphragm, $\overline{c_{app}}$ drops to 17 m/s. With the exception of the measurements between location 4 and 5, there is a good correspondence between $\overline{c_{app}}$ and c_{ff}.

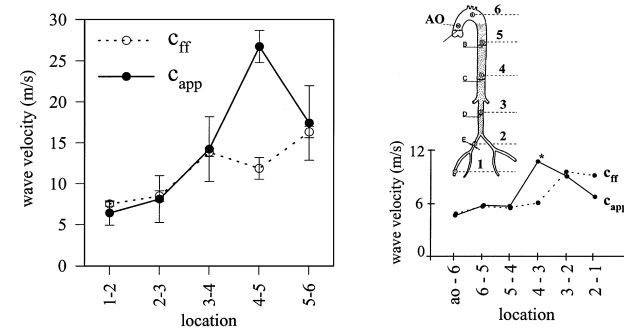

Fig. 2. *Hydraulic model*. Left: comparison of $\overline{c_{app}}$ with c_{ff} between two successive measuring locations in the aorta. Right: measuring locations in the study of Latham et al. (1985) and comparison of $\overline{c_{app}}$ with c_{ff} in vivo derived from pressure measurements between successive locations under control conditions (after Latham et al., 1985).

For the more distal locations, the input impedance increases. Z_0, calculated from the higher frequencies (6–10 Hz), yields values of 0.053, 0.073, 0.084, 0.287, 0.495 and 0.781 mmHg/(ml/s) at the six locations. These values are used for the separation of the waves into their forward and backward components, shown in Fig. 3 for locations 1, 4 and 6.

3.2. Mathematical model simulations

The input impedance patterns for the low (LC), normal (NC) and high compliance (HC) model are given in Fig. 4. In the LC model, the minimum of the input impedance modulus is at 6.98 Hz. With an average wave velocity of 9.30 m, the distance to an apparent reflection point is $x = 33$ cm. For the NC model, average wave speed is 4.16 m/s, $f_{min} = 3.08$ Hz and $x = 34$ cm and for the HC model, $x = 34$ cm for an average wave speed of 1.86 m/s and $f_{min} = 1.35$ Hz.

The average of the high frequencies (5–10 Hz) of c_{app} is shown in Fig. 5, together with the foot-to-foot wave velocity and the Moens-Korteweg wave velocity. Both c_{ff} and $\overline{c_{app}}$ overestimate the Moens-Korteweg wave velocity at most locations, but the overestimation is highest in the LC model and lowest in the HC model. At the distal end, close to the terminal reflection point, both approximations overestimate the Moens-Korteweg velocity by a factor 2 or more.

The separation of the pressure wave into its forward and reflected component is given in Fig. 6 for the three models. If the timing of the retrograde waves is studied using the foot of the retrograde wave, the first retrograde wave appears at the most proximal location. However, using the zero reference level to study the time delay (Δt) between incident and reflected wave, a delay of 0.05 s is found in the LC model, corresponding to a reflection site

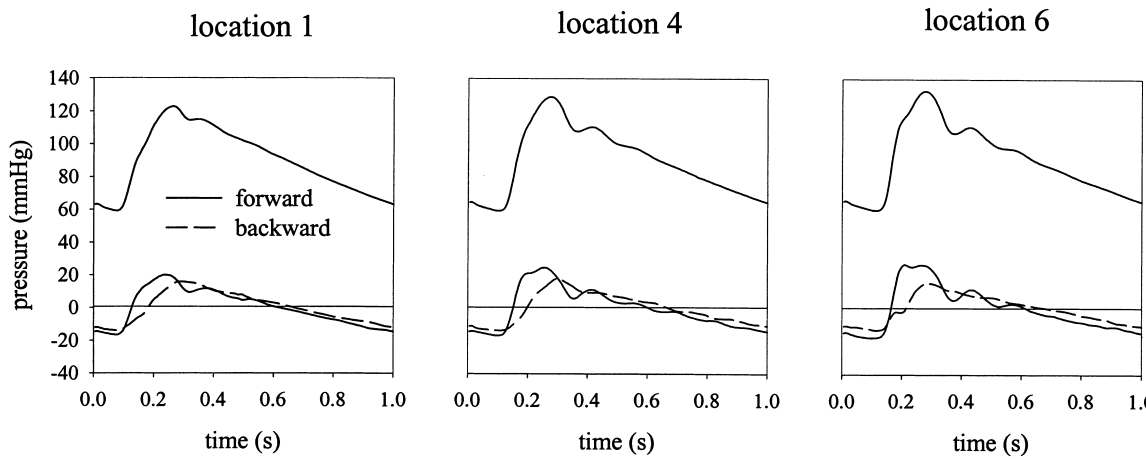

Fig. 3. *Hydraulic model.* Measured pressure and linear separation into a forward (P_f) and reflected (P_b) wave at three locations along the aorta (1: $x = 1$ cm; 4: $x = 30$ cm; 6: $x = 48$ cm distal from the heart).

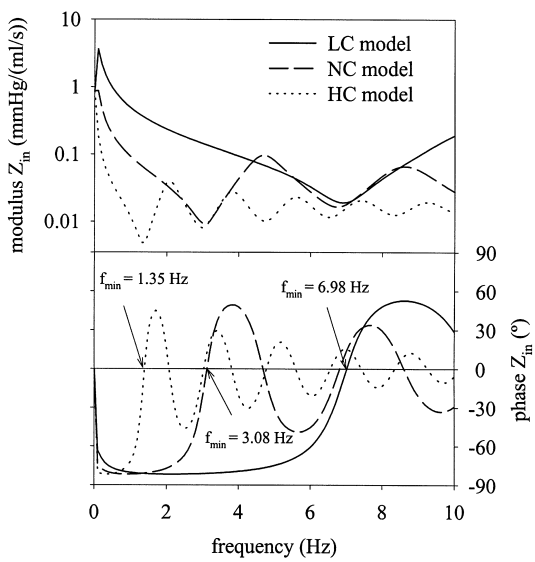

Fig. 4. *Mathematical model.* Input impedance modulus (top) and phase angle (bottom) for the low (0.32 ml/mmHg), normal (1.6 ml/mmHg) and high (8 ml/mmHg) compliance tapered aorta model, with indication of the frequency of the first minimum of the impedance modulus.

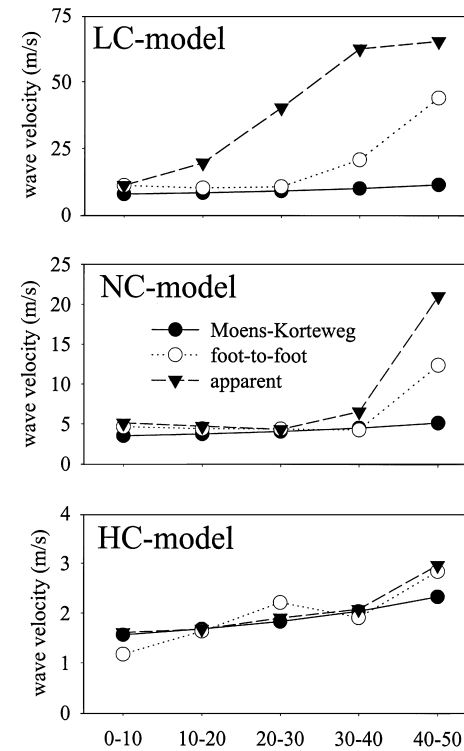

Fig. 5. *Mathematical model.* Calculated foot-to-foot and apparent phase velocity $\overline{c_{app}}$(5–10 Hz) compared to the actual Moens-Korteweg wave velocity in the low (top), normal (middle) and high (bottom) compliance model.

at 23 cm (calculating the distance with the average wave velocity). For the NC model and HC model, $\Delta t = 0.14$ and 0.38 s and the reflections are found at 30 and 35 cm, respectively. Computing incident and reflected wave at $x = 30$ cm, there again exists a time delay corresponding to distances of 11, 11 and 9 cm for the LC, NC and HC model, respectively.

The number of segments in the tapering model influences wave reflection indices such as x_{refl} (Fig. 7). For 2 segments (each 25 cm long), x_{refl} is about 34 cm. With increasing number, x_{refl} reaches a minimum for 3–5 segments and a stable value for $N > 100$. This value is slightly lower than the value found for two segments. The tapering angle has a more outspoken effect. For $\theta = 0°$ (straight tube), x_{refl} is found at the distal end of the tube ($x = 50$ cm). x_{refl} decreases rapidly and tends toward an asymptotic value of 25 cm. For physiological tapering angles (0–1.5°), x_{refl} varies between 50 and 30 cm.

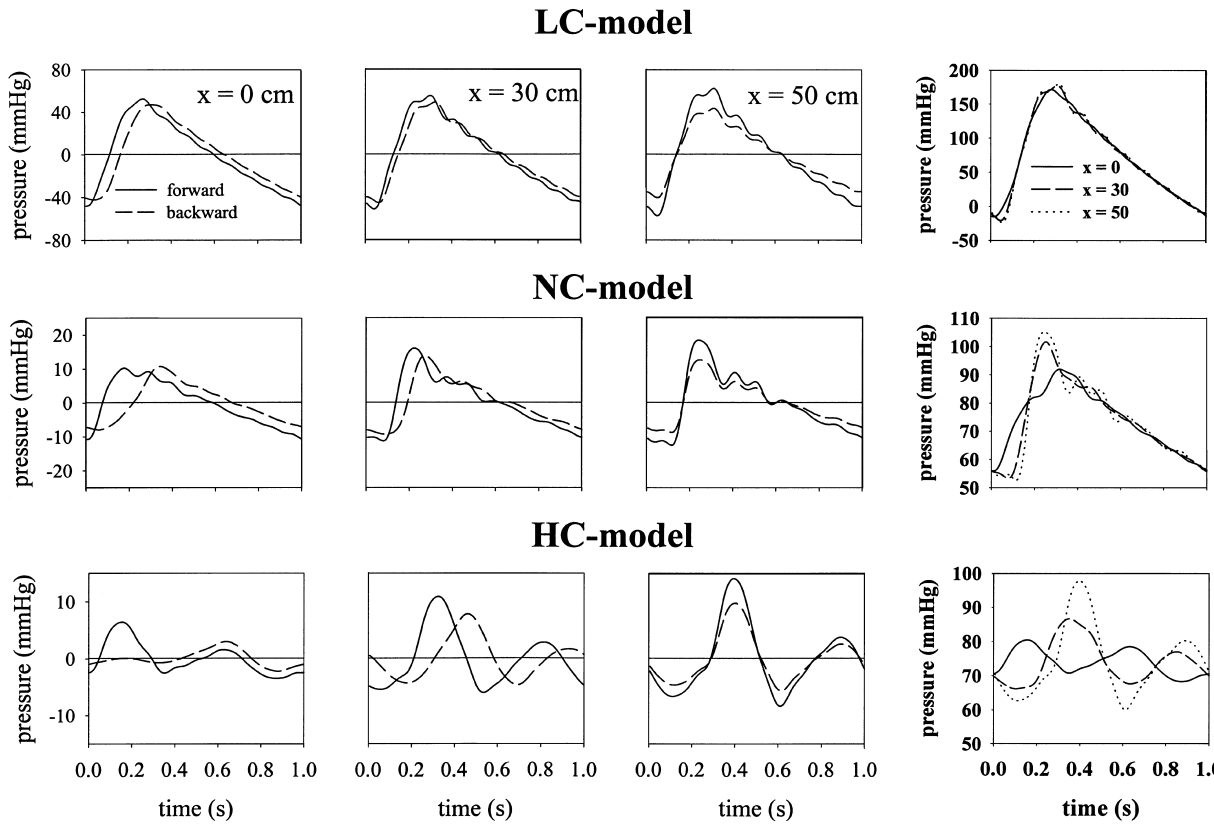

Fig. 6. *Mathematical model*. Computed pressure (right panels) and linear separation into a forward (P_f) and reflected (P_b) wave at three locations (three left panels) along the tapered aorta model ($x = 0$, 30 and 50 cm) for the low (upper panels), normal (middle panels) and high (lower panels) compliance model.

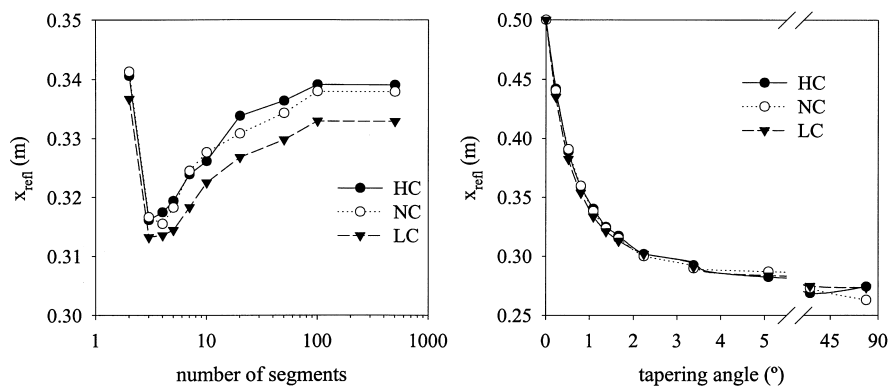

Fig. 7. *Mathematical model*. Parameter study showing the effect of an increased number of segments (left panel) and of tapering angle (right panel) on distance to the apparent reflection site. Results are given for the low, normal and high compliance model.

4. Discussion

The idea of the existence of an important reflection site in the human aorta, at the level of the renal arteries, was introduced by Latham et al. (1985). This conclusion was based on time and frequency domain analysis of pressure waves measured at six locations along the aorta. In this study, we repeated their work using a hydraulic arterial network model. Our similar experimental observations (discrepancy between foot-to-foot and apparent phase velocity at the level of the diaphragm; reflection site at $x = 40$ cm predicted by the quarter-wavelength formula) apparently confirm their findings. As our model provided extra information, we could calculate the propagation of forward and reflected waves along the aorta. However, instead of revealing a clear discrete reflection point, this analysis showed a continuous reflection along the aorta. In order to unravel these apparently conflicting results

and to investigate the role of arterial tapering, we did a mathematical model simulation on a simplified model of the tapering aorta.

Latham et al. (1985) formulated several arguments to support the existence of a discrete reflection site at the renal arteries: (i) c_{app} reached a minimum at higher frequencies (= closer to a reflection site) in the segment more proximal than distal to the renal arteries; (ii) the amplification of harmonics (associated with the presence of a reflection site) was strongest proximal to the renal arteries under control conditions; (iii) angiograms showed a significant reduction in diameter of the aortic segment crossing the diaphragm; (iv) the local reflection coefficient was relatively high (0.43) (Latham et al., 1985). These arguments, however, cannot account for our hydraulic model: (i) the minima in c_{app} are situated between 5 and 7 Hz for all aortic segments, with no clear distinction between the segments proximal or distal to the renal arteries; (ii) the amplification of the first four pressure harmonics is maximal at the distal end of the aorta; (iii) in the hydraulic model, the tapering of the aorta is smooth with a linear reduction in diameter from the ascending to the abdominal aorta; (iv) computation of the local reflection coefficient in the tapering aorta from Z_0 in the segment proximal (0.29 mmHg/(ml/s)) and distal (0.49 mmHg/(ml/s)) to the renal arteries gives $(0.49 - 0.29)/(0.49 + 0.29) = 0.26$. This value is an upper limit, as no parallel branches are taken into account in the computation of the local reflection coefficient. Therefore, we cannot explain the wave reflection phenomena at the level of the diaphragm by a discrete reflection point at the level of the renal arteries, caused by a sudden reduction in aortic diameter.

Differences between in vivo measurements of Latham et al. and our experimental findings may be partly due to factors related to the experimental setting, influencing wave reflection. The compliance in our hydraulic model was relatively low, giving less damping and higher wave velocities (see Fig. 2). We also fixed the model at discrete locations to avoid disturbing oscillations. We did not directly study the impact of this fixation, but it is likely that it generated only minor secondary effects seen the physiological morphology of pressure and flow waves (Segers et al., 1998). Other differences are the termination of the arteries in our model (a linear hydraulic resistance), branching angles, mechanical arterial properties, etc.

The time course of the forward and retrograde wave at the six locations along the aorta, obtained after splitting total pressure, is not clear. For a single discrete reflection site, the backward wave is first generated at this location, and then propagates in the upstream direction. This is not the case in the hydraulic model: taking the foot of the backward wave as a reference, it appears that a backward wave is generated as the forward wave arrives, suggesting continuous reflection along the tapering aorta. The pattern is even more confusing using the zero pressure as a reference line: the time delay between incident and reflected wave practically does not change from location 1 to location 6. The presence of a continuous reflection is consistent with classic wave reflection theory, that predicts wave reflection with any change in the characteristic impedance (Milnor, 1989). In the tapering aorta, Z_0 increases continuously.

The effect of aortic tapering on wave reflection is studied by means of a mathematical model, using a simplified geometry of the aorta, and for three different stiffness values covering the range of arterial elasticity observed in normal and pathological conditions (pulse wave velocity between 1.9 and 9.3 m/s). As in the hydraulic model, the aortic diameter varies in a linear way, with a constant tapering angle along the aorta (1.1°). Our only goal, justifying this simple geometry, is to demonstrate the effect of tapering on wave reflection, and on indices characterising wave reflection. It is shown that when the quarter-wavelength formula and the input impedance minimum are used to calculate a reflection point in the tapering tube, an "apparent" reflection point is found. For our simulations this reflection point is located about 33 cm distal to the aortic valve, practically independent of compliance. This distance is close to the level of the renal arteries.

The simplified model of the tapering aorta cannot explain the discrepancy between c_{ff} and $\overline{c_{\mathrm{app}}}$ observed in the hydraulic model and in vivo by Latham et al. (1985). This discrepancy is probably due to high local reflections, arising from the short branches to the abdominal organs. In our mathematical model, local wave reflection is high at the distal end, and here also $\overline{c_{\mathrm{app}}}$ overestimated c_{ff} by a factor 2 or more. The overestimation is higher in the low compliance model, and the influence of the local distal reflection is present over a longer section.

Calculating incident and reflected waves in the tapering model, the interpretation of the timing of incident and reflected waves depends on which reference point on the backward wave is used, and on the compliance of the model. Taking the foot of the backward wave, the pattern of a continuous reflection is found in the normal and low compliance models, with the backward wave occurring first in the most proximal part of the tube. In the high compliance model, the backward wave first occurs at the downstream end and propagates towards the inlet. However, using the zero pressure as a reference line, a clear delay between incident and reflected wave is present in all models. This delay corresponds to the distance to a reflection site. For the tube inlet, the so found reflection site is close to the "apparent" reflection site found using the quarter-wavelength formula. Both distances should be close, as the equations behind both approaches are derived within the same conceptual model, where the arterial tree is seen as a single tube with a discrete terminal

reflection site. At $x = 30$ cm, near the "apparent" reflection site, there is again a time delay between the incident and reflected wave. This delay corresponds to a new distance of 9 to 11 cm. Using the linear wave separation theory at $x = 30$ cm, the remaining 20 cm of the tapering tube is again abstracted as a single tube model, again yielding a new "apparent" reflection site and a new "effective" length of about 60% of its total length.

In the mathematical model, tapering is modelled as a stepwise reduction in diameter, and it is expected that the number of segments affects wave reflection and derived indices. We estimated x_{frel} using 2 to 500 segment elements. Note that $N = 1$ corresponds to a straight tube, where $x_{\mathrm{refl}} = 50$ cm. x_{refl} is highest for $N = 2$, but already within 1 cm of the value found for $N > 100$. The shortest distance is found for N between 5 and 8. A more important determinant of x_{refl} is the tapering angle. Changing θ affects both geometric and elastic tapering, as the latter is determined by the elasticity modulus and by the ratio of local wall thickness to diameter. Changes in θ from 0 to 2° (increase in geometric and elastic taper) shift x_{refl} from the distal tube end ($x = 50$ cm) to $x = 30$ cm.

In summary, we believe that measured in vivo aortic wave reflection indices are the result of at least two interacting phenomena: a continuous wave reflection due to arterial tapering, and local reflections arising from branches at the level of the diaphragm. The continuous reflection is hidden in the input impedance pattern. Using the quarter-wavelength formula or the classical wave separation theory, it appears as a reflection coming from a single discrete site, confusingly also located at the level of the diaphragm. Therefore, the quarter-wavelength formula and the linear wave separation theory should be used with caution to identify wave reflection zones in the presence of tapering, i.e. in most mammalian arteries.

Acknowledgements

This research is funded by a post-doc grant of the Flemish institute for the Promotion of the Scientific-Technological Research in Industry (IWT/OZM/960250) and by a Concerted Action Program of the University of Gent, supported by the Flemish government (GOA 95003).

References

Avolio, A., 1980. Multi-branched model of the human arterial system. Medical and Biological Engineering and Computing 18, 709–718.

Berger, D., Li, J., Laskey, W., Noordergraaf, A., 1993. Repeated reflection of waves in the systemic arterial system. American Journal of Physiology 264, H269–H281.

Campbell, K., Lee, C.L., Frasch, H.F., Noordergraaf, A., 1989. Pulse reflection sites and effective length of the arterial system. American Journal of Physiology 256, H1684–H1689.

Franklin, S., Weber, M., 1994. Measuring hypertensive cardiovascular risk: the vascular overload concept. American Heart Journal 128, 793–803.

Karamanoglu, M., Fenely, M., 1997. On-line synthesis of the human ascending aortic pressure pulse from the finger pulse. Hypertension 30, 1416–1424.

Karamanoglu, M., Gallagher, D., Avolio, A., O'Rourke, M., 1994. Functional origin of reflected pressure waves in a multibranched model of the human arterial system. American Journal of Physiology 267, H1681–H1688.

Latham, R., Westerhof, N., Sipkema, P., Rubal, B., Reuderink, P., Murgo, J., 1985. Regional wave travel and reflections along the human aorta: a study with six simultaneous micromanometric pressures. Circulation 72, 1257–1269.

Milnor, W., 1989. Hemodynamics, 2nd edition. Williams & Wilkins, Baltimore, Maryland, USA.

Murgo, J., Westerhof, N., Giolma, J., Altobelli, S., 1980. Aortic input impedance in normal man: relationship to pressure wave forms. Circulation 62, 105–116.

O'Rourke, M.F., 1967. Pressure and flow waves in systemic arteries and the anatomical design of the arterial system. Journal of Applied Physiology 23, 139–149.

O'Rourke, M.F., Avolio, A.P., 1980. Pulsatile flow and pressure in human systemic arteries. Studies in man and in a multibranched model of the human systemic arterial tree. Circulation Research 46, 363–372.

Segers, P., Dubois, F., De Wachter, D., Verdonck, P., 1998. Role and relevancy of a cardiovascular simulator. Cardiovascular Engineering 3, 48–56.

Segers, P., Stergiopulos, N., Verdonck, P., Verhoeven, R., 1997. Assessment of arterial network models. Medical and Biological Engineering and Computing 35, 729–736.

Westerhof, N., Bosman, F., De Vries, C.J., Noordergraaf, A., 1969. Analog studies of the human systemic arterial tree. Journal of Biomechanics 2, 121–143.

Westerhof, N., Elzinga, G., Sipkema, P., 1971. An artificial arterial system for pumping hearts. Journal of Applied Physiology 31, 776–781.

Westerhof, N., Sipkema, P., Van Den Bos, G., Elzinga, G., 1972. Forward and backward waves in the arterial system. Cardiovascular Research 6, 648–656.

Womersley J. R., 1957. An elastic tube theory of pulse transmission and oscillatory flow in mammalian arteries. Wright Air Development Centre, Technical Report WADC-TR 56-614.